Supporting Information

Structural reconstruction of $BiPbO_2Br$ nanosheets for electrochemical CO_2 reduction to formate

Gaoming Sun,‡[ab] Chong Zou,‡[c] Wen Sun,[ab] Ying Fang,[ab] Shuijian He,[d] Yana Liu,[ab] Jiguang Zhang,[ab] Yunfeng Zhu*[ab] and Jun Wang*[ab]

[a]College of Materials Science and Engineering, Nanjing Tech University, 30 South Puzhu Road, Nanjing 211816, China.

E-mail: jun22@njtech.edu.cn; yfzhu@njtech.edu.cn

[b]Jiangsu Collaborative Innovation Centre for Advanced Inorganic Function Composites, Nanjing Tech University, Nanjing 211816, China.

[c]School of Chemistry and Molecular Engineering, Nanjing Tech University, Nanjing 211816, China.

[d]Co-Innovation Centre of Efficient Processing and Utilization of Forest Resources, College of Materials Science and Engineering, Nanjing Forestry University, Nanjing 210037, China.

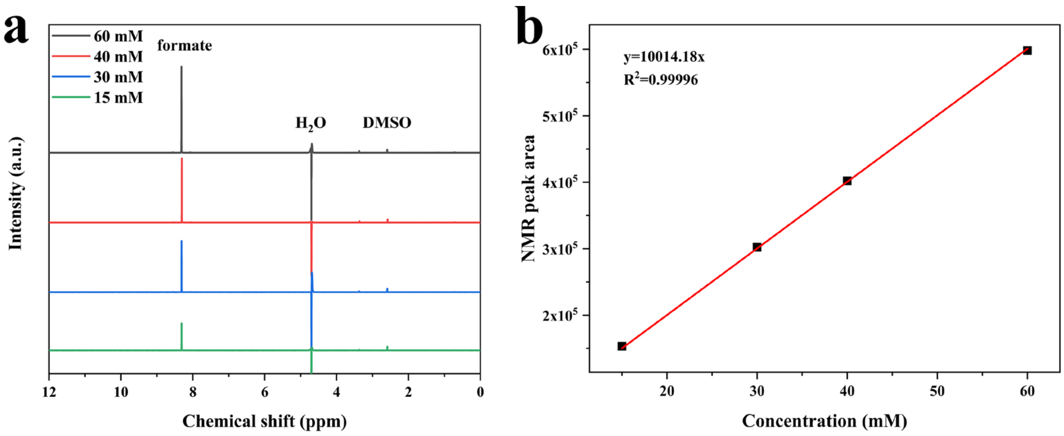

Fig. S1. (a) ^{1}H NMR spectra of formate with different concentration. (b) The corresponding calibration curve.

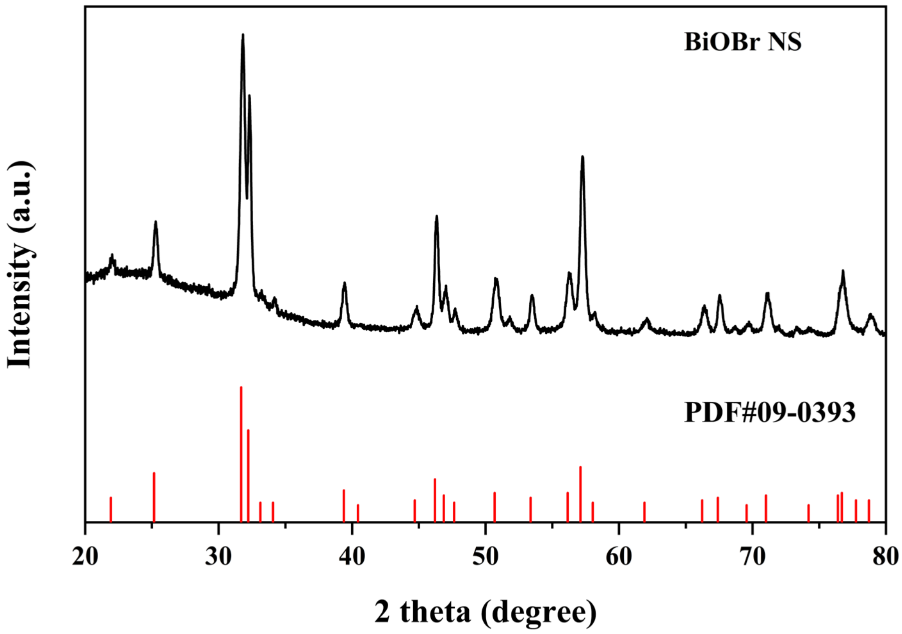

Fig. S2. XRD pattern of BiOBr NS.

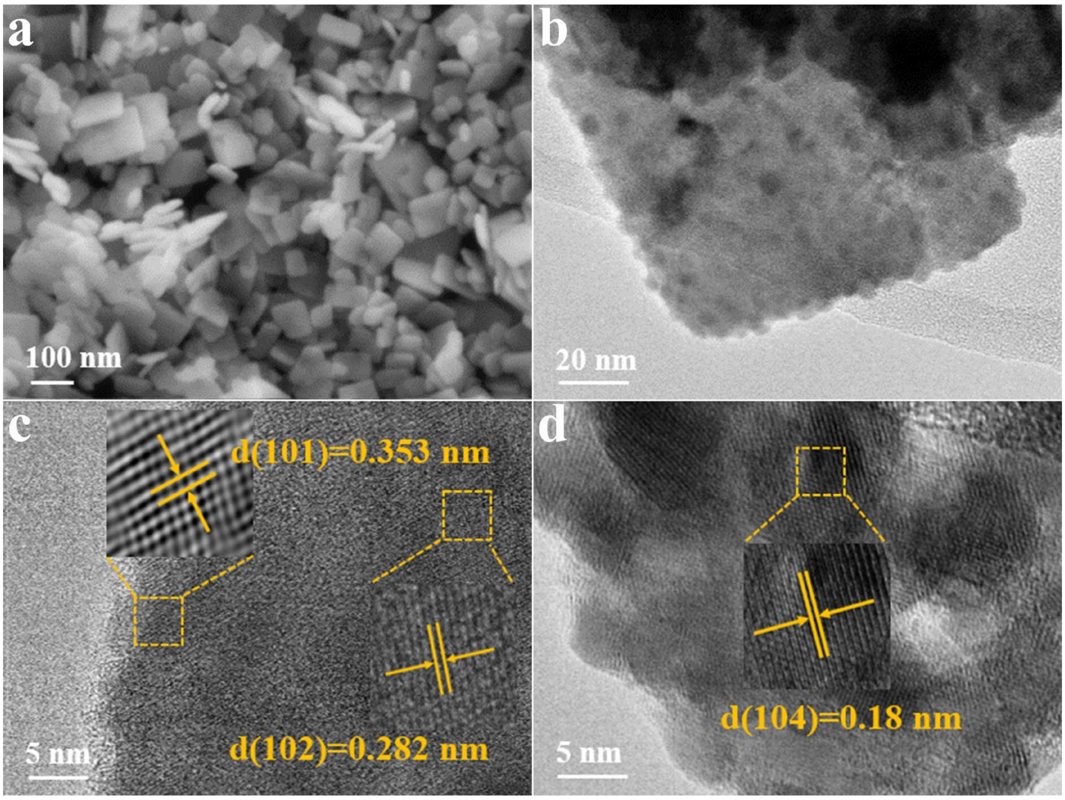

Fig. S3. (a) SEM, (b) TEM and (c-d) HRTEM images of BiOBr NS.

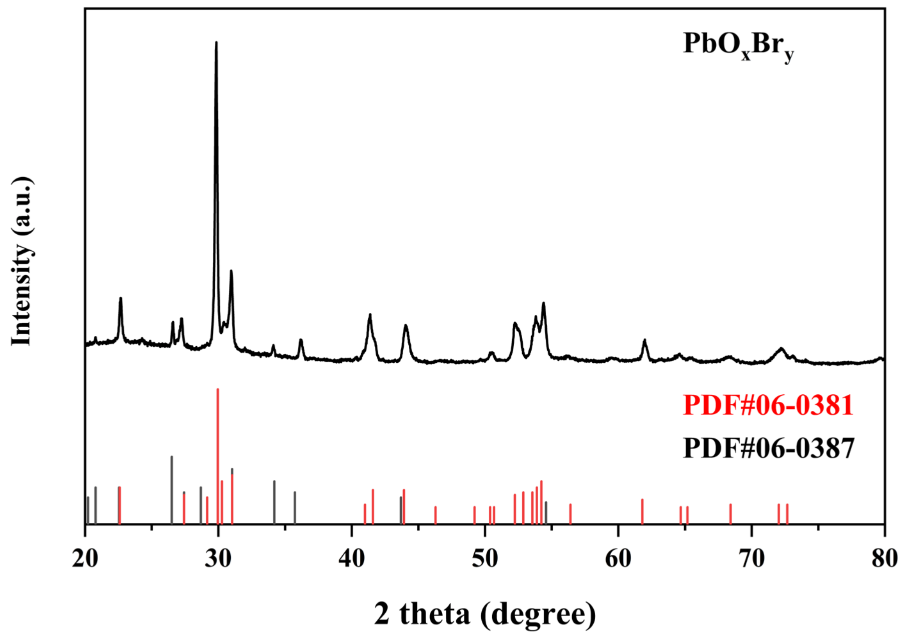

Fig. S4. XRD pattern of PbO_xBr_y.

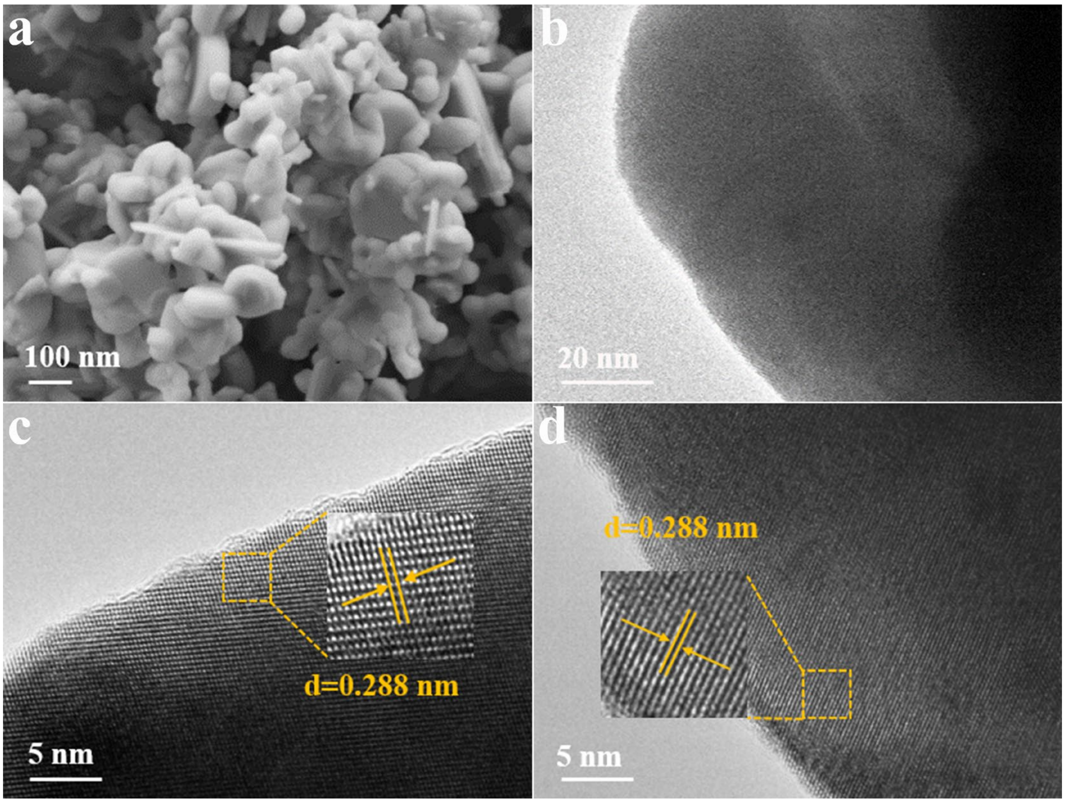

Fig. S5. (a) SEM, (b) TEM and (c-d) HRTEM images of PbO_xBr_y.

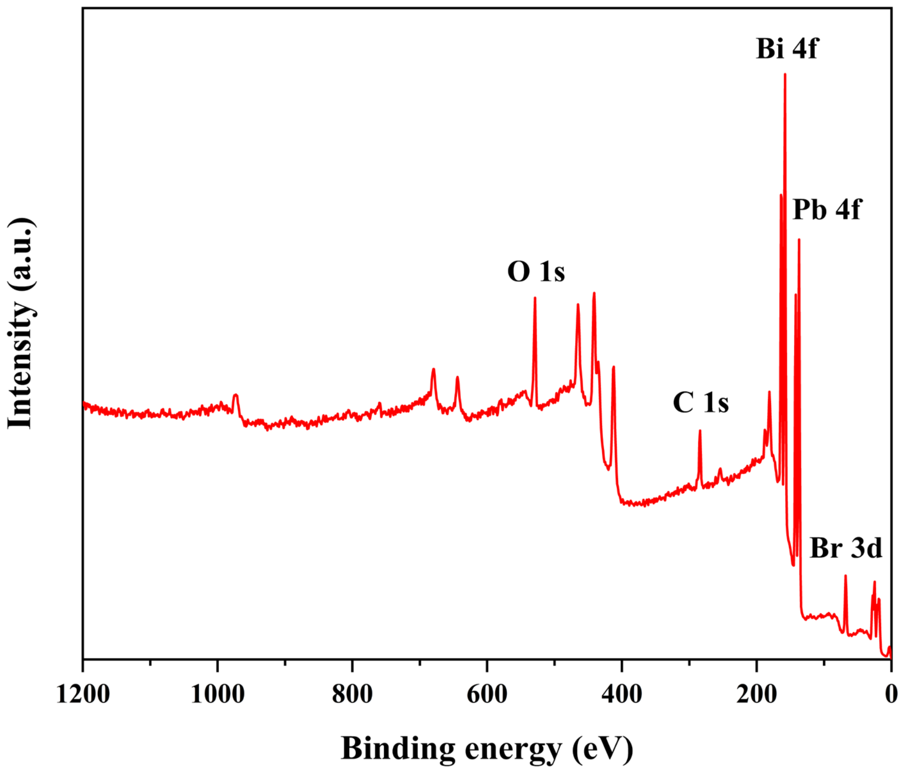

Fig. S6. XPS survey spectrum of $BiPbO_2Br$.

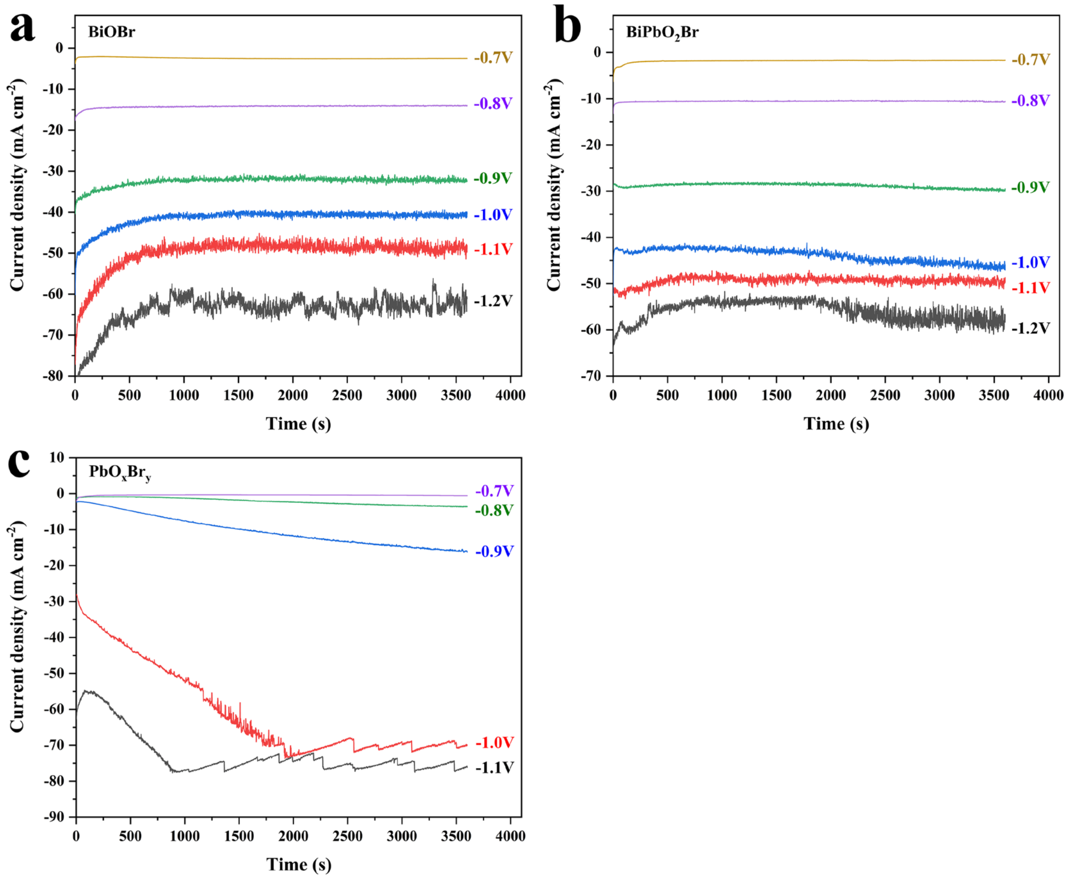

Fig. S7. The controlled electrolysis at different potentials over (a) BiOBr, (b) $BiPbO_2Br$ and (c) PbO_xBr_y in CO_2-saturated 0.5 M $NaHCO_3$.

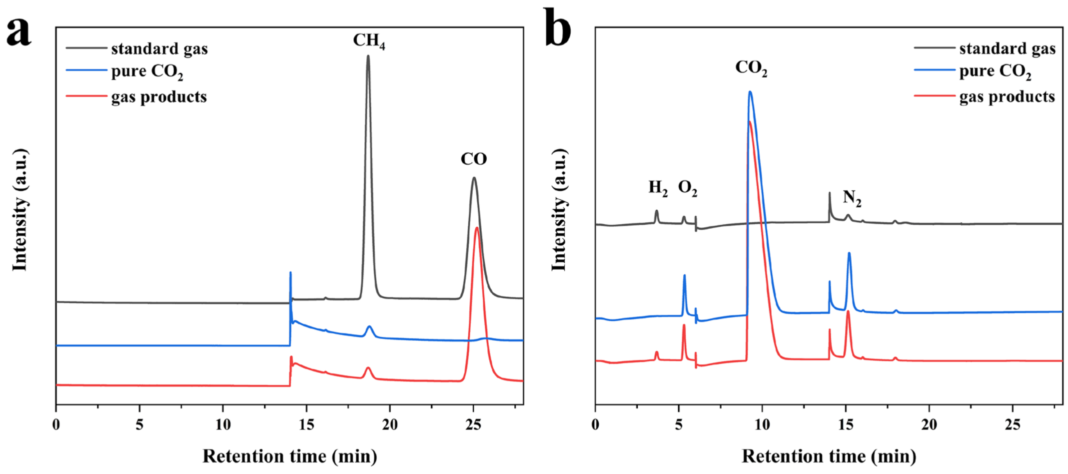

Fig. S8. GC FID (a) and TCD (b) spectra for determining CO and H_2 in gaseous products over $BiPbO_2Br$ at -0.9 V. Notably, the standard gas and pure CO_2 were also measured for comparison.

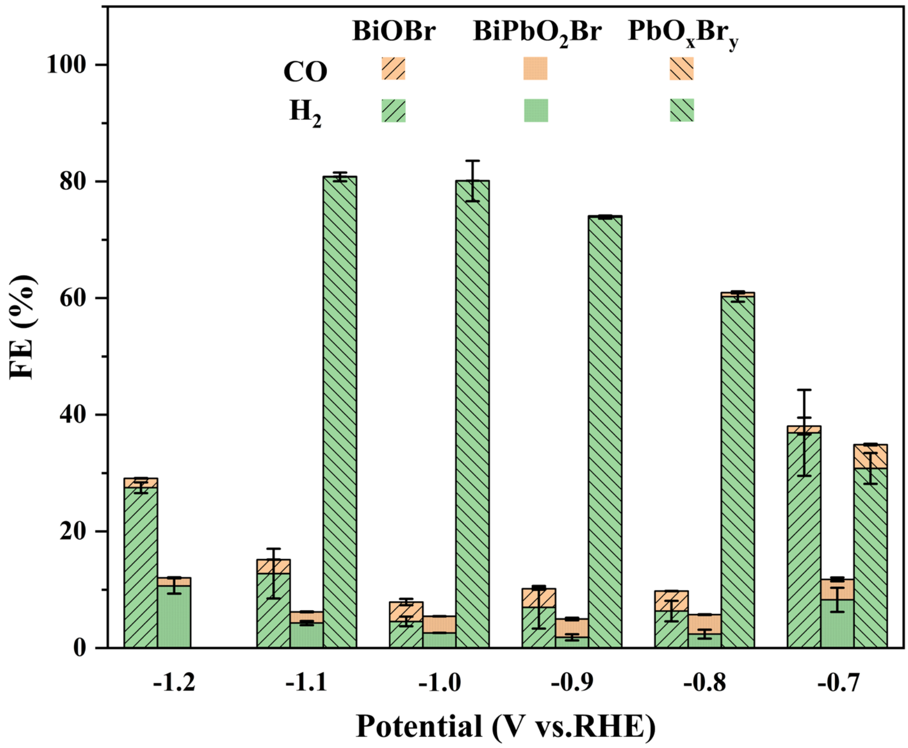

Fig. S9. Faradaic efficiency of CO and H_2 over BiOBr, $BiPbO_2Br$ and PbO_xBr_y at different potentials.

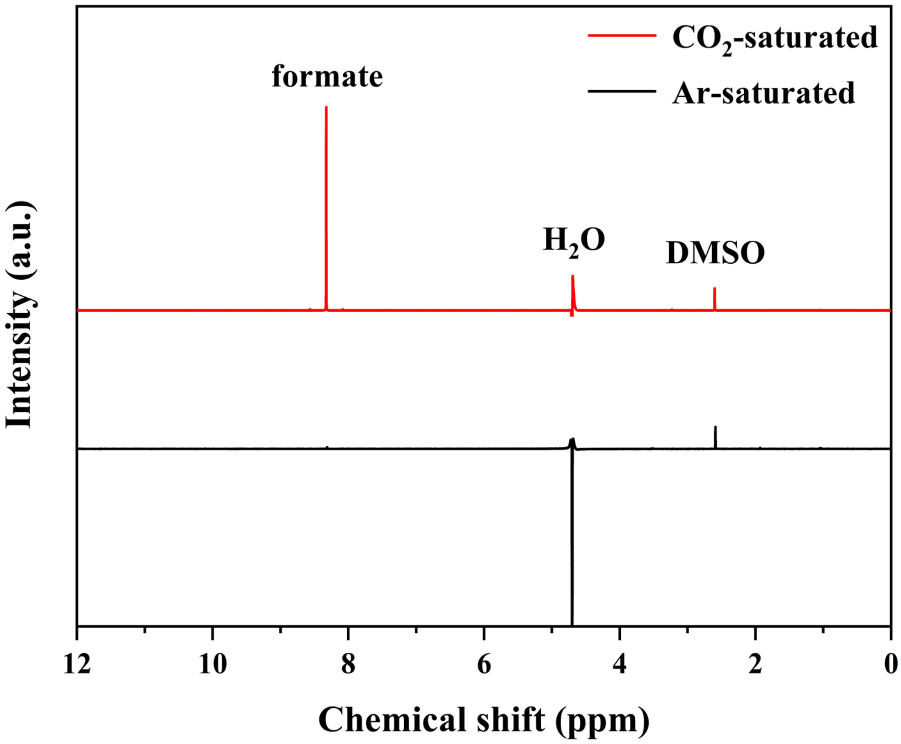

Fig. S10. ^{1}H NMR spectra of CO_2 or Ar-saturated 0.5 M $NaHCO_3$ solution after 1 h electrolysis over $BiPbO_2Br$.

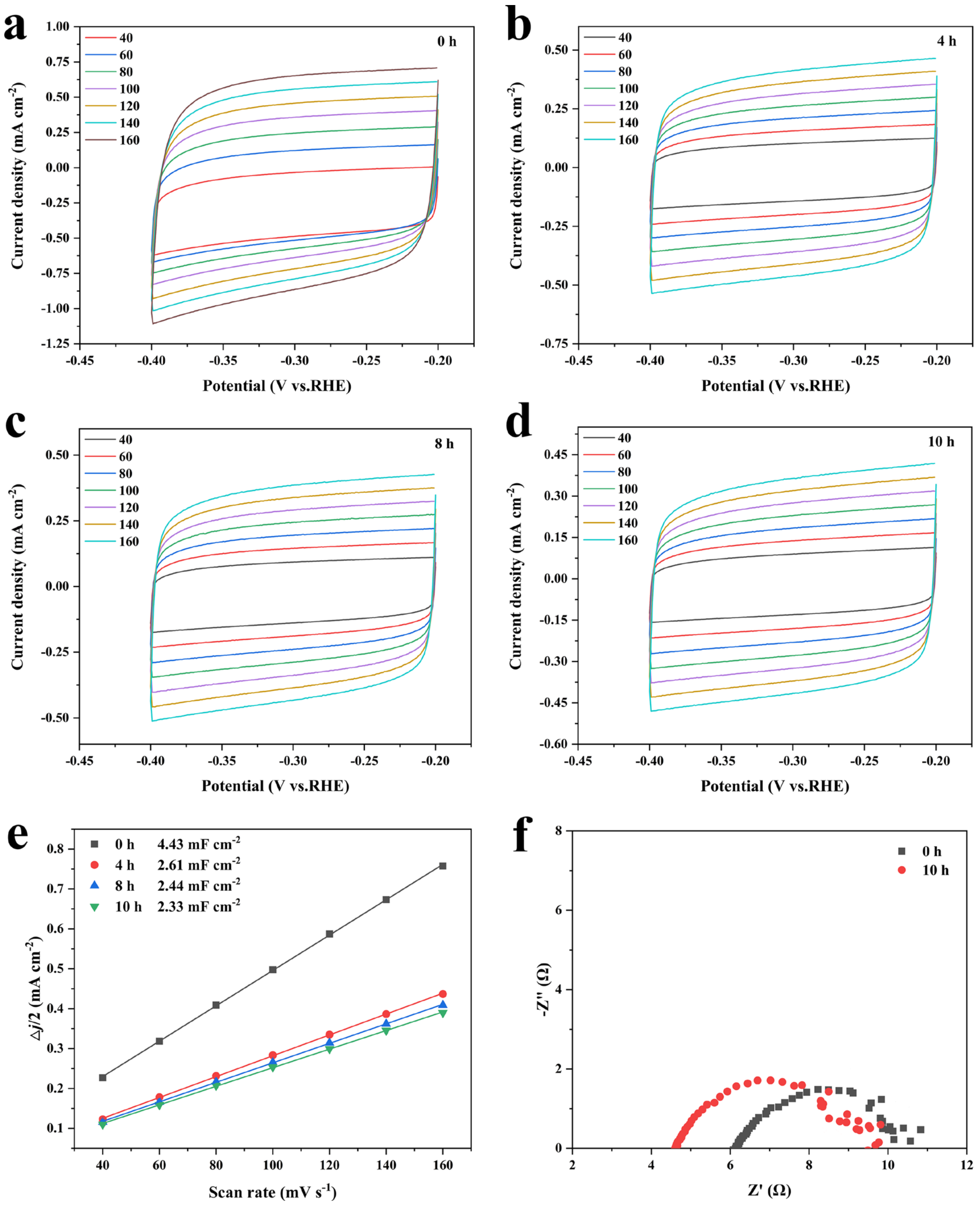

Fig. S11. (a-d) CV curves at different scan rates for $BiPbO_2Br$ with varied electrolysis time, (e) the according charging current density plotted against scan rates, and (f) EIS spectra of $BiPbO_2Br$ before and after the long-term chronoamperometric test.

It is found that the C_{dl} of $BiPbO_2Br$ electrode is gradually decreased with the preceding of chronoamperometric test, implying the decrease of ECSA. However, the EIS spectra reveal that the contact resistance of the electrode is obviously reduced, suggesting the increased conductivity after the test, which should be contributed to the increased current density during the chronoamperometric test.

Table S1. Comparison of CO_2RR-to-formate performance of recently reported Bi or Pb-based electrocatalysts in H-type cell.

Catalyst	**Electrolyte**	**FE (formate, %)**	**E (V vs.RHE)**	**$j_{formate}$ (mA cm^{-2})**	**Ref.**
$BiPbO_2Br$	0.5 M $NaHCO_3$	96.6	-0.9	26	This work
		93.1	-1.0	40	
Bi-OAm-300	0.5 M $KHCO_3$	97.1	-0.9	31.1	1
SOR Bi@C NPs	0.5 M $KHCO_3$	95	-0.99	10.5	2
BiOCl	0.5 M $KHCO_3$	92	-0.9	28.63	3
Pd-$Pb_3(CO_3)_2(OH)_2$	0.1 M $KHCO_3$	96.5	-1.2	13	4
3D Bi-ene-A/CM	0.5 M $KHCO_3$	96.02	-0.88	21.21	5
Bi-Cu	0.5 M $KHCO_3$	94.37	-0.91	27.85	6
Bi-PNS	0.5 M $KHCO_3$	95	-1.0	45	7
Bi/CB	0.5 M $KHCO_3$	94	-0.9	16.7	8
Pits-Bi	0.1 M $KHCO_3$	94.9	-1.0	17.2	9
BiOCl-derived	0.5 M $KHCO_3$	92	-0.9	10.5	10
Bi/Bi_2O_3-CP	0.5 M $KHCO_3$	90.3	-0.87	32.4	11
BBNS	0.5 M $NaHCO_3$	>92	-0.89	11.5	12
Bi-Sn	0.1 M $KHCO_3$	93.9	-1.0	9.3	13
f-Bi_2O_3	0.1 M $KHCO_3$	87	-1.2	20.9	14
BiPb	0.5 M $NaHCO_3$	91.86	-0.96	15.56	15

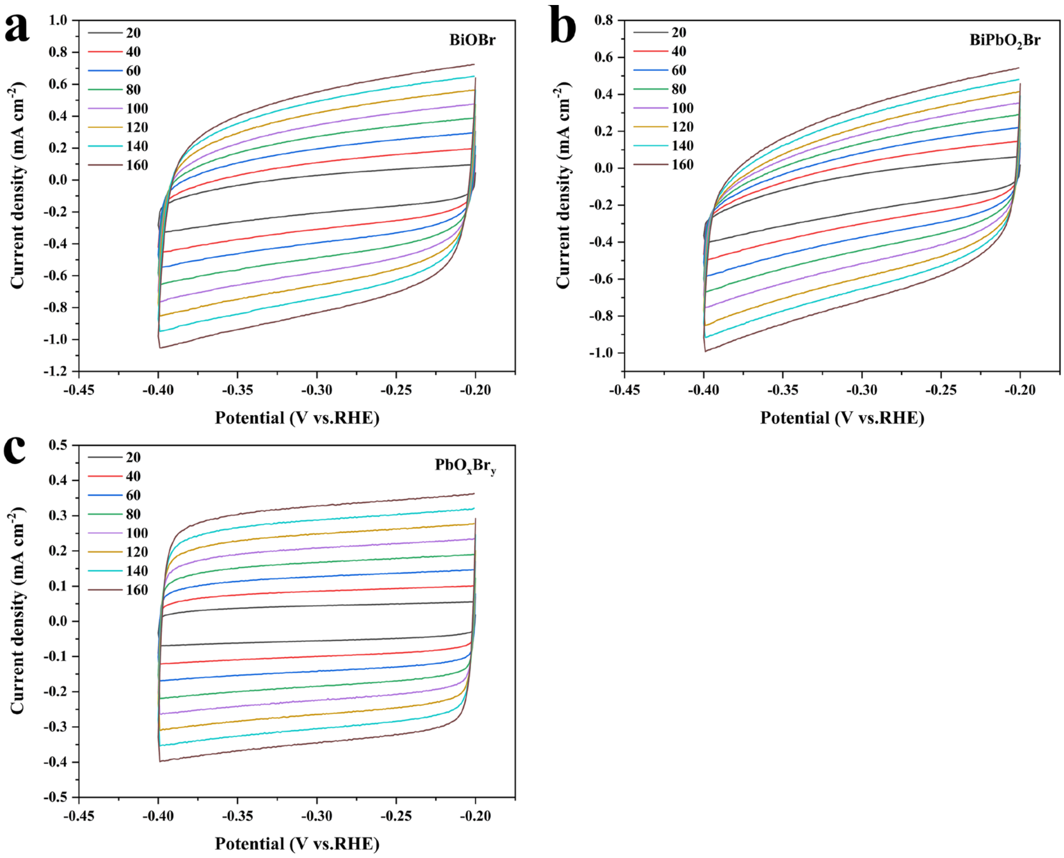

Fig. S12. CV curves of (a) BiOBr, (b) $BiPbO_2Br$ and (c) PbO_xBr_y with different scan rates.

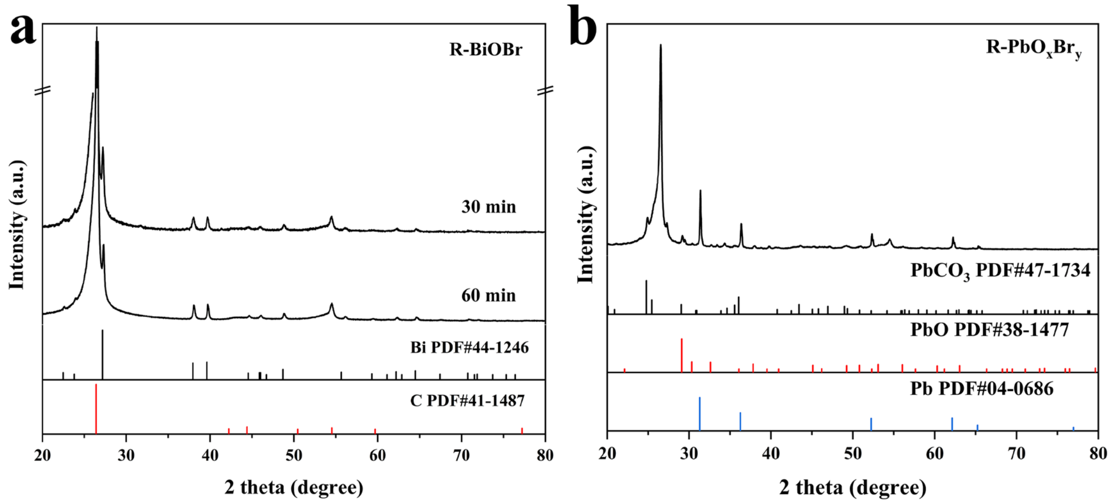

Fig. S13. XRD patterns of BiOBr and PbO_xBr_y after electroreduction.

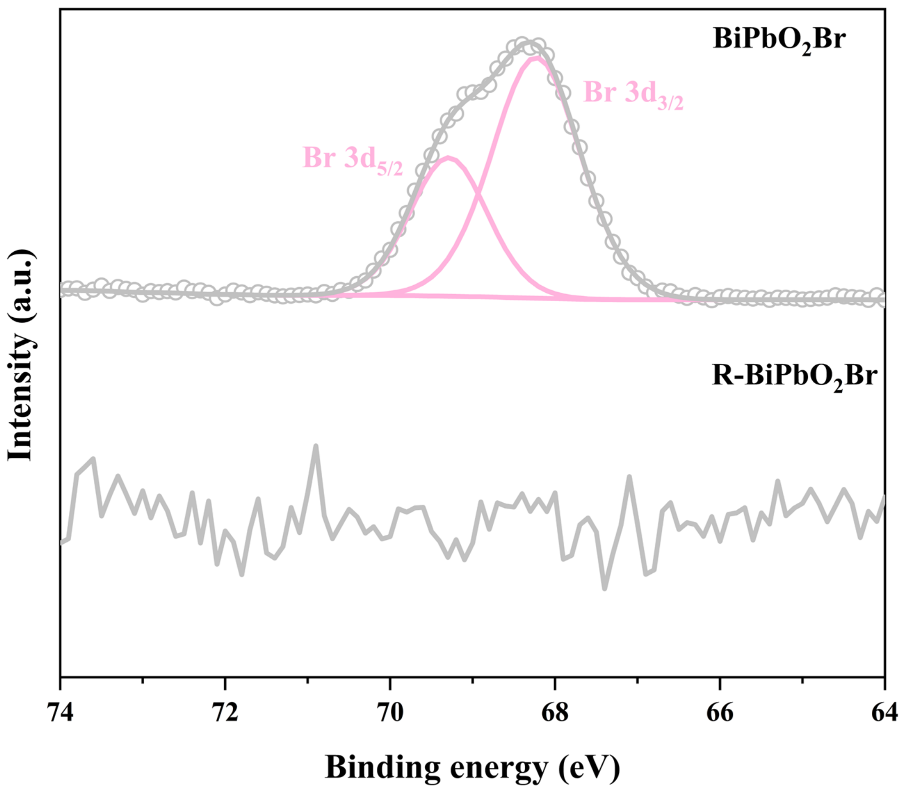

Fig. S14. Br 3d XPS spectra of $BiPbO_2Br$ before and after electroreduction.

Reference

1. H. Zheng, G. Wu, G. Gao and X. Wang, The bismuth architecture assembled by nanotubes used as highly efficient electrocatalyst for CO_2 reduction to formate, *Chem. Eng. J.*, 2021, **421**, 129606.
2. S. Liu, Y. Fan, Y. Wang, S. Jin, M. Hou, W. Zeng, K. Li, T. Jiang, L. Qin, Z. Yan, Z. Tao, X. Zheng, C. Shen, Z. Liu, T. Ahmad, K. Zhang and W. Chen, Surface-Oxygen-Rich Bi@C Nanoparticles for High-Efficiency Electroreduction of CO_2 to Formate, *Nano Lett.*, 2022, **22**, 9107-9114.
3. Y. Zhou, P. Yan, J. Jia, S. Zhang, X. Zheng, L. Zhang, B. Zhang, J. Chen, W. Hao, G. Chen, Q. Xu and B. Han, Supercritical CO_2-constructed intralayer $[Bi_2O_2]^{2+}$ structural distortion for enhanced CO_2 electroreduction, *J. Mater. Chem. A*, 2020, **8**, 13320-13327.
4. W. Huang, Y. Wang, J. Liu, Y. Wang, D. Liu, J. Dong, N. Jia, L. Yang, C. Liu, Z. Liu, B. Liu and Q. Yan, Efficient and Selective CO_2 Reduction to Formate on Pd-Doped $Pb_3(CO_3)_2(OH)_2$: Dynamic Catalyst Reconstruction and Accelerated CO_2 Protonation, *Small*, 2022, **18**, e2107885.
5. Y. C. He, D. D. Ma, S. H. Zhou, M. Zhang, J. J. Tian and Q. L. Zhu, Integrated 3D Open Network of Interconnected Bismuthene Arrays for Energy-Efficient and Electrosynthesis-Assisted Electrocatalytic CO_2 Reduction, *Small*, 2022, **18**, e2105246.
6. L. Peng, Y. Wang, Y. Wang, N. Xu, W. Lou, P. Liu, D. Cai, H. Huang and J. Qiao, Separated growth of Bi-Cu bimetallic electrocatalysts on defective copper foam for highly converting CO_2 to formate with alkaline anion-exchange membrane beyond $KHCO_3$ electrolyte, *Appl. Catal., B*, 2021, **288**, 120003.
7. Z. L. Yu, S. Q. Wu, L. W. Chen, Y. C. Hao, X. Su, Z. Zhu, W. Y. Gao, B. Wang and A. X. Yin, Promoting the Electrocatalytic Reduction of CO_2 on Ultrathin Porous Bismuth Nanosheets with Tunable Surface-Active Sites and Local pH Environments, *ACS Appl. Mater. Interfaces*, 2022, **14**, 10648-10655.
8. S. Q. Wu, Y. C. Hao, L. W. Chen, J. Li, Z. L. Yu, Z. Zhu, D. Liu, X. Su, L. Hu, H. Z. Huang and A. X. Yin, Modulating the electrocatalytic CO_2 reduction performances of bismuth nanoparticles with carbon substrates with controlled degrees of oxidation, *Nanoscale*, 2021, **13**, 20091-20097.
9. Y. Yuan, Q. Wang, Y. Qiao, X. Chen, Z. Yang, W. Lai, T. Chen, G. Zhang, H. Duan, M. Liu and H. Huang, In Situ Structural Reconstruction to Generate the Active Sites for CO_2 Electroreduction on Bismuth Ultrathin Nanosheets, *Adv. Energy Mater.*, 2022, **12**, 2200970.
10. P. Liu, H. Liu, S. Zhang, J. Wang and C. Wang, Effects of thicknesses and sizes of BiO_X nanoplates precursors on derived Bi nanosheets for efficient CO_2 electroreduction, *J. CO_2 Util.*, 2021, **51**, 101643.
11. D. Wu, G. Huo, W. Chen, X.-Z. Fu and J.-L. Luo, Boosting formate production at high current density from CO_2 electroreduction on defect-rich hierarchical mesoporous Bi/Bi_2O_3 junction nanosheets, *Appl. Catal., B*, 2020, **271**, 118957.
12. J. Zhu, J. Fan, T. Cheng, M. Cao, Z. Sun, R. Zhou, L. Huang, D. Wang, Y. Li and Y. Wu, Bilayer nanosheets of unusual stoichiometric bismuth oxychloride for potassium ion storage and CO_2 reduction, *Nano Energy*, 2020, **75**, 104939.
13. Z. Wu, H. Wu, W. Cai, Z. Wen, B. Jia, L. Wang, W. Jin and T. Ma, Engineering Bismuth-Tin Interface in Bimetallic Aerogel with a 3D Porous Structure for Highly Selective Electrocatalytic

CO_2 Reduction to HCOOH, *Angew. Chem., Int. Ed.*, 2021, **60**, 12554-12559.
14. T. Tran-Phu, R. Daiyan, Z. Fusco, Z. Ma, R. Amal and A. Tricoli, Nanostructured β-Bi_2O_3 Fractals on Carbon Fibers for Highly Selective CO_2 Electroreduction to Formate, *Adv. Funct. Mater.*, 2019, **30**, 1906478.
15. X. Zhang, X. Jiao, Y. Mao, X. Zhu, H. Kang, Z. Song, X. Yan, X. Yan, C. Han, L. Cui, K. Zhang and J. Qiao, A BiPb bimetallic electrode for highly selective CO_2 conversion to formate, *Sep. Purif. Technol.*, 2022, **300**, 121848.